(Received 10 January 2025, Accepted 11 April 2025, Scheduled 19 April 2025)

Multi-Objective Optimization Design of Surface-Mounted and Interior Hybrid Permanent Magnet Synchronous Motor

Aikang Xu*, Chaozhi Huang, Bo Yi, Fangrong Wang, and Zhifeng Liu

Jiangxi University of Science and Technology, China

ABSTRACT: Aiming at the problems of low ability of speed control by means of magnetic field weakening of surface-mounted permanent magnet synchronous motor and large torque pulsation and more magnetic leakage of interior permanent magnet synchronous motor, a new structure of surface-mounted and interior hybrid permanent magnet synchronous motor is proposed. By establishing a finite element model of the motor and simulating it, and comparing the electromagnetic characteristic curves of the motor after simulation with those of the surface-mounted permanent magnet synchronous motor and interior permanent magnet synchronous motor, the results show that the motor proposed in this paper has the advantages of both good weak magnetic performance and higher torque output. In the optimization of surface-mounted and interior hybrid permanent magnet synchronous motor, with the goal of achieving high torque value, low torque ripple, and low cogging torque, a multi-objective optimization strategy combining genetic algorithm (GA) optimized back-propagation (BP) network and non-dominated sorting genetic algorithm (NSGA-II) is adopted. Firstly, a comprehensive sensitivity analysis of the degree of influence of the design variables on the optimization objective is carried out, based on which the parameter variables are stratified, and then an accurate prediction model of the parameter variables and optimization objective is established by using GA-BP. Finally, the multi-objective optimization is carried out by NSGA-II, and the optimal design is selected from the generated Pareto frontiers. After comparing the electromagnetic performances of the motor before and after optimization, the effectiveness as well as the superiority of the multi-objective optimization design method is verified.

1. INTRODUCTION

Permanent magnet synchronous motors are widely used in electric vehicles, wind turbines, compressors, etc. because of their high power factor, efficiency, and torque density [1–3].

According to the locations of rotor permanent magnets, permanent magnet synchronous motors can be divided into surface-mounted permanent magnet synchronous motors and interior permanent magnet synchronous motors. The permanent magnet inside the rotor of a interior permanent magnet synchronous motor is not easy to demagnetize because it is protected by the pole shoe, and the reluctance torque generated by the asymmetric rotor magnetic circuit structure is also conducive to the improvement of the motor's overload capacity and power density and helps the flux-weakening speed regulation. However, there are problems such as the mechanical strength of the part near the magnetic isolation bridge is slightly weaker [4], and the cogging torque and torque ripple cause vibration and noise in the motor [5, 6]. Surface-mounted permanent magnet synchronous motors have high power density despite poor flux-weakening performance. The permanent magnets of this motor are in contact with the air gap, and the size, shape, and magnetizing method of the permanent magnets will directly affect the distribution of the magnetic field in the air gap, which has a large impact on the performance of the motor [7].

As the air-gap magnetic flux density is an important performance indicator of permanent magnet synchronous motors, it is of great significance to optimize its waveform and numerical value. Some scholars have made slots on the magnetic poles of surface-mounted permanent magnet synchronous motors to make the fundamental harmonic of the air-gap magnetic flux density a sine wave, thus making the back electromotive force closer to a sine wave [8]. In addition, structures such as eccentric surface-mounted magnetic poles and nonuniform Halbach permanent magnet arrays have also been proposed. The results show that these structures can all generate a highly sinusoidal air-gap magnetic field and increase the content of the fundamental wave frequency of the air-gap magnetic flux density, thereby increasing the electromagnetic torque and reducing the torque ripple [9, 10].

In addition to the innovative design of motor topology, multi-objective optimization is also one of the important methods to improve the performance of motors [11]. Some scholars use genetic algorithm, simulated annealing algorithm, and particle swarm optimization algorithm to optimize the motor, because these algorithms have strong global search ability and do not depend on the initial value. The difficulty of local optimization has been solved well, but individual algorithms do not take the influence weights between parameters into account, which is prone to the fact that the optimization effect is not obvious. Ref. [12] proposes a sensitivity analysis of the rotor geometric parameters of an internal permanent magnet synchronous motor, which leads to a significant improvement in the performance of the optimized motor. Refs. [13, 14] used a hierarchical optimization strategy based on the results of the sensitivity

* Corresponding author: Aikang Xu (3350377927@qq.com).

analysis to reduce the interference between the parameters and then used an optimization algorithm combining the response surface model and NSGA-II to improve the torque and reduce the pulsations of the motor. Refs. [15, 16] used response surface methodology to establish an agent model of a permanent magnet synchronous motor and combined it with particle swarm algorithm to optimize the torque as well as other properties of the motor. In addition, agent models such as random forest [17, 18], deep learning [19], and support vector machine [20] have been applied in the optimization of motors and achieved significant results.

In this paper, a finite element simulation model of a surface-mounted and interior hybrid permanent magnet synchronous motor is developed and compared with the electromagnetic characteristic curves of the conventional interior and surface-mounted permanent magnet synchronous motors. Based on the proposed comprehensive sensitivity analysis method of the influence of design variables on the electromagnetic performance of the motor, the design variables are stratified by sensitivity, then the accurate prediction model of the design variables and optimization target is obtained by using the genetic algorithm (GA) optimization back-propagation (BP). The optimal solution is obtained by using the global optimization of the prediction model with NSGA-II. Finally, the superior performance of the optimized motor is verified by comparing the parameters such as airgap magnetic flux densities and electromagnetic torques of the motor before and after optimization.

2. MOTOR STRUCTURE AND WORKING PRINCIPLE

Surface-mounted and interior hybrid permanent magnet synchronous motor (SIHPMSM) combines the characteristics of surface-mounted permanent magnet synchronous motor (SPMSM) and interior permanent magnet synchronous motor (IPMSM), which is achieved through a series magnetic circuit between the surface-mounted permanent magnets and interior permanent magnets. The design parameters of this motor are shown in Table 1, and the structure is shown in Fig. 1.

TABLE 1. Parameters of the SIHPMSM.

Parameter	Unit	Value
Outer diameter of stator	mm	150
Outer diameter of rotor	mm	83.2
Air-gap length	mm	0.5
Shaft length	mm	115
Rated speed	r/min	1500
Poles/slots		4/12
Rated voltage	V	380
Number of conductors per slot		88

In Fig. 1, the thickness of the surface-mounted pole in the rotor part is H_2; its corresponding angle on the circumference is α_2; the width of the interior pole is W_1; the thickness is H_1; its distance from the air gap is L_1; and the magnetic barrier angle inside the rotor is α_1. Taking into account the mechanical

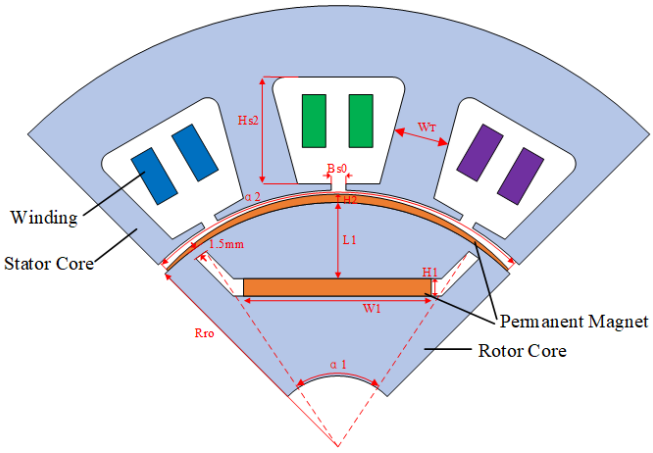

FIGURE 1. SIHPMSM structure.

strength of the rotor as well as its performance requirements, the width of the magnetic bridge is set at 1.5 mm, and R_{ro} is the rotor outer diameter (excluding the thickness of the surface-mounted pole). B_{s0}, W_T, and H_{s2} are the slot width, tooth width, and slot depth of the stator part, respectively. The thickness of the surface-mounted pole in the figure is thin, close to the air gap, as an auxiliary pole. On the one hand, the magnetic field it generates can change part of the magnetic circuit of the magnetic isolation bridge and reduce the magnetic leakage of the motor. On the other hand, it can alter the distribution of the air-gap magnetic field, increase the proportion of the fundamental wave of the air-gap magnetic flux density, make the air-gap magnetic flux density more sinusoidal, and then reduce the torque ripple of the motor, making its output torque smoother. The main magnetic flux of the motor is generated by the interior magnetic poles, which act as the main magnetic poles and contribute the most to the output torque of the motor, and at the same time make the motor have better flux-weakening performance.

3. MOTOR CHARACTERIZATION

3.1. No-Load Characteristics

In order to analyze the electromagnetic characteristics of the SIHPMSM, the SIHPMSM with surface-mounted permanent magnets and interior permanent magnets is compared with the SPMSM with equal-thickness surface-mounted permanent magnet and the IPMSM with only interior permanent magnets. In this paper, the stator part parameters of the three motors are the same. The surface-mounted poles of the SPMSM and the surface-mounted poles of the SIHPMSM are equal in dosage and have the same pole-arc coefficients, and the structural shapes of the interior permanent magnets of the IPMSM are almost the same as those of the SIHPMSM. Fig. 2 shows the magnetic density and the distribution of magnetic lines of force of the three kinds of motors under no-load condition. For SIHPMSM and SPMSM, parallel magnetization can produce a more sinusoidal air-gap magnet flux density waveform than radial magnetization, and the cogging torque is also lower; therefore, parallel magnetization is used for the surface-mounted

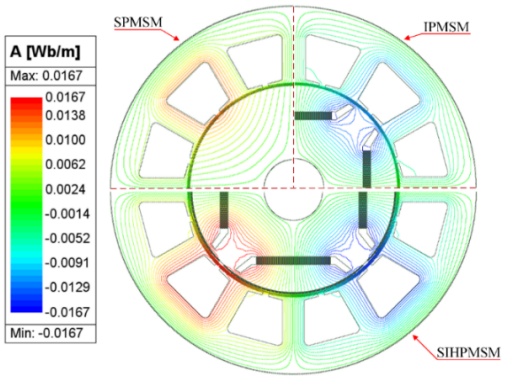

FIGURE 2. Cloud chart of the magnetic field line distribution of the motor under no-load condition.

permanent magnets of these two motors. From Fig. 2, it can be seen that the magnetic leakage of SIHPMSM and SPMSM is less, but there is magnetic leakage in the magnetic barrier part of the rotor of IPMSM, and in the non-saturated state of the core of the motor, the interior permanent magnets and surface-mounted permanent magnets of the SIHPMSM are connected in series in the magnetic circuit in such a structure, which can make the motor have more effective magnetic flux.

The air-gap flux density can reflect the torque output capability of the motor, and the distortion of the air-gap flux density waveform will exacerbate the torque ripple of the motor, bringing vibration as well as noise. Fig. 3 shows the radial air-gap flux density waveforms of the three motors under one cycle when they are in the no-load state, and in order to better analyze their sinusoidality, Eq. (1) is used to calculate the harmonic distortion rate (THD) of the air-gap flux density. The air-gap flux density distortion rates of SPMSM and IPMSM are 37.1% and 33.34%, respectively, while the SIHPMSM has the lowest distortion rate of 16.06%, and the lower air-gap flux density harmonic distortion rate makes the SIHPMSM have lower torque ripple and vibration noise than the other two motors.

$$THD = \frac{\sqrt{\sum_{k=2}^{\infty} B_k^2}}{B_1} \times 100\% \tag{1}$$

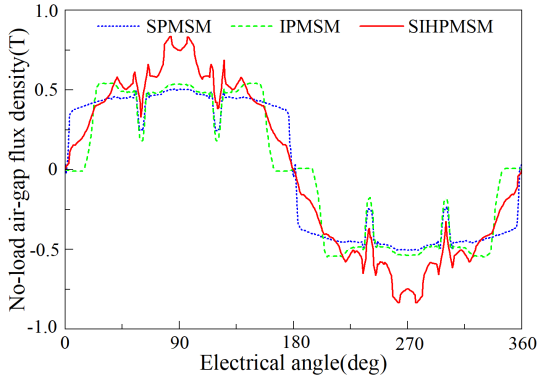

FIGURE 3. Waveform of the air-gap magnetic flux density.

where k is the harmonic order, and B_1 and B_k are the amplitude of the fundamental wave and the amplitude of the kth harmonic component of the no-load radial air-gap magnetic flux density, respectively.

The degree of sinusoidality of the back electromotive force (back-EMF) waveform will have a direct impact on the operating performance of the motor, and it is of great significance to make the back-EMF of the motor close to the sinusoidal waveform. Fig. 4 shows the back-EMF waveforms of the three motors, where the harmonic distortion rate of the IPMSM is 27.08%; the SPMSM has the largest harmonic distortion rate of 34.23%; and the back-EMF of the SIHPMSM is the most sinusoidal, having the lowest harmonic distortion rate of 9.4%.

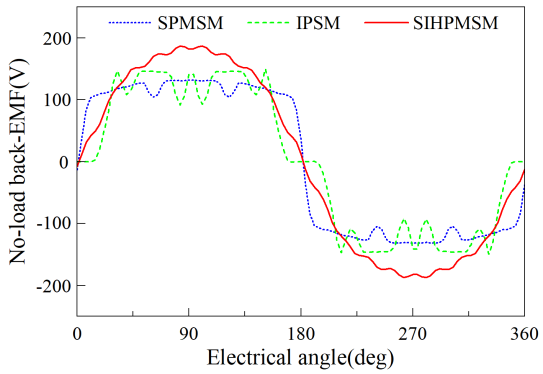

FIGURE 4. Waveform of the no-load back-EMF.

3.2. Load Characterization

The output torque characteristics of the motor, as an important index to measure the performance of permanent magnet synchronous motor, should be fully considered in the design of the motor. Fig. 5 shows the curves of the average value of the output torque of three motors at an industrial frequency current with a current RMS value of 5A about the variation of the internal power factor angle (the angle between the phase no-load back EMF and the phase current). Because the q-axis inductance L_q and d-axis inductance L_d of the SPMSM are equal, its

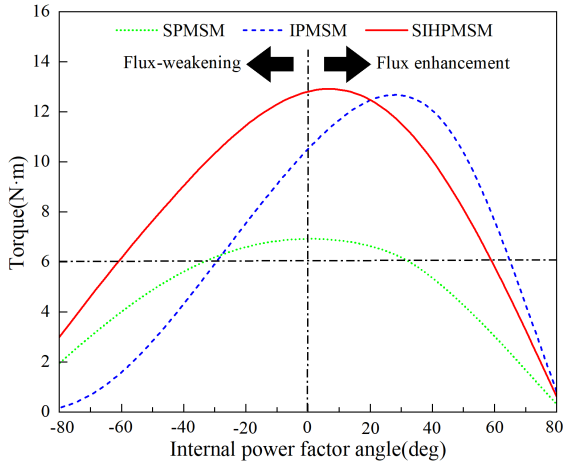

FIGURE 5. Average torque under different internal power factor angles.

output torque is maximum when the internal power factor angle is equal to 0, which is mainly the permanent magnet torque; the q-axis and d-axis inductances of the interior permanent magnet synchronous motor are unequal, in which $L_d < L_q$, so that the motor's output torque includes the reluctance torque, so that the IPMSM can make use of reluctance torque to keep the motor in the weak magnetism state at the time when the d-axis current $i_d < 0$. The internal power factor angle ψ of the SIHPMSM at the maximum output torque is located between the SPMSM and IPMSM, and the motor combines the advantages of high sinusoidal air-gap magnetic flux density of the SPMSM and better flux-weakening performance of the IPMSM. Because the thickness of the surface-mounted poles is thinner than that of the interior poles, the output torque value of the SPMSM is smaller than that of the other two motors. The maximum output torque value of the SIHPMSM is slightly higher than that of the IPMSM, but its range of outputting a large torque is wider than that of both the IPMSM and SPMSM, and thus the SIHPMSM is stronger in terms of its torque output capability.

4. MULTI-OBJECTIVE OPTIMIZATION DESIGN OF SIHPMSM

4.1. Determination of Optimization Objectives and Design Variables

Average torque, torque ripple, and cogging torque, as important indicators of motor characteristics, should be fully considered in the design of the motor. Larger average torque can make the motor have higher power density, while too much torque ripple and cogging torque can lead to vibration and noise of the motor. In order to make the performance of SIHPMSM superior, the average output torque T_{avg}, torque ripple T_{rip}, and peak-to-peak value of cogging torque T_{cog} of the motor are taken as the optimization objectives, and the average output torque of the motor is increased as much as possible while making the motor's torque ripple and cogging torque smaller. Eqs. (2) and (3) are the formulas for the average output torque and torque ripple of the motor, respectively.

$$T_{avg} = T_{pm} + T_{re} = \frac{3}{2}P\left[\psi_{pm} i_q + (L_d - L_q) i_d i_q\right] \quad (2)$$

In Eq. (2), T_{pm} and T_{re} denote the permanent magnet torque and reluctance torque of the motor, respectively; ψ_{pm} denotes the magnetic flux generated by the permanent magnets; P is the number of pole pairs; L_d and L_q denote the d-axis and q-axis inductances; and i_d and i_q denote the d-axis and q-axis currents, respectively.

$$T_{rip} = \frac{T_{\max} - T_{\min}}{T_{avg}} \times 100\% \quad (3)$$

In Eq. (3), $T_{\max}$ is the maximum value of output torque, $T_{\min}$ the minimum value of output torque, and T_{avg} the average value of output torque.

The multi-objective optimization function is determined as follows:

$$f(x_i)_{\min} = \omega_1 \frac{T^*_{avg}(x_i)}{T_{avg}(x_i)} + \omega_2 \frac{T_{rip}(x_i)}{T^*_{rip}(x_i)} + \omega_3 \frac{T_{cog}(x_i)}{T^*_{cog}(x_i)} \quad (4)$$

$$\min x_i \le x_i \le \max x_i, \quad i = 1, 2, 3, \ldots, 10 \quad (5)$$

Constraints:

$$\begin{cases} T_{avg} \ge 13\,\mathrm{N \cdot m} \\ T_{rip} \le 12\% \\ T_{cog} \le 1.1\,\mathrm{N \cdot m} \end{cases} \quad (6)$$

In Eqs. (4) and (5), x_i are 10 parameter variables; $T^*_{avg}(x_i)$, $T^*_{rip}(x_i)$, and $T^*_{cog}(x_i)$ are the initial values of average torque, torque ripple, and cogging torque of the SIHPMSM, respectively; and $T_{avg}(x_i)$, $T_{rip}(x_i)$, and $T_{cog}(x_i)$ are the average torque, torque ripple, and cogging torque after optimization, respectively. ω_1, ω_2, and ω_3 are the weight coefficients of the three optimization objectives, and $\omega_1 + \omega_2 + \omega_3 = 1$. There is no uniform standard for the values of weight coefficients, and in this paper, the three weight coefficients are taken to be 0.3, 0.4, and 0.3, respectively.

In this paper, the structure of the proposed SIHPMSM will be optimized and designed, and the related design variables have been marked in Fig. 1. The design process of this motor consists of two main parts. The first part is the design of the stator core structure and the determination of the winding related parameters, and the second part is the design of the rotor structure including the magnetic barrier structure and the determination of the size of permanent magnets. In order to reduce the harmonic content of the stator magnetomotive force, the stator winding type is a distributed winding. A suitable stator tooth width can enhance the magnetic flux density in the stator tooth section, so that the motor can effectively utilize the magnetic field energy to generate torque; an appropriate slot depth can reduce the resistance of the windings, thus reducing the copper loss and improving the efficiency of the motor; the width of the slot openings will have a significant impact on the distortion of the air-gap magnetic flux density of the motor, so the three parameters W_T, H_{s2}, and B_{s0} are selected as the design variables of the stator part of the SIHPMSM. For the rotor part, the outer diameter of the rotor and the angle of the air magnetic barrier, the length, width, and position of the interior permanent magnets, the thickness of the surface-mounted poles, and the pole arc coefficient are parameters that have a great impact on the motor's performance like the output torque. Therefore, seven parameters, R_{ro}, α_1, W_1, H_1, L_1, H_2, and α_2, are selected as the design variables for this part. Table 2 shows the range of values for the ten design variables.

4.2. Optimization Structure Sensitivity Analysis

From Table 2, it can be seen that the multi-objective optimal design of SIHPMSM is a nonlinear and multidimensional optimal design problem. The problem involves strong coupling between the motor structural parameters, which together affect the optimization objective. If ten variables are optimized at the same time, it will bring a huge amount of computation, which greatly increases the difficulty of optimization design. Therefore, this paper reduces the number of experiments and computational complexity by analyzing the sensitivity of the optimization objectives to the design variables and then stratifying the design variables according to the sensitivity analysis results. In the process of multi-objective optimization, it is necessary to

TABLE 2. Design variables and range of values.

Design Variables	Unit	Variation Ranges
L_1	mm	11.3–13.5
H_1	mm	2.7–3.4
W_1	mm	29–34.5
α_1	deg	49–54
H_2	mm	0.8–1.05
α_2	deg	84–89
W_T	mm	8.1–9.8
B_{s0}	mm	2.4–3.1
R_{ro}	mm	40–42
H_{s2}	mm	16–18

measure the correlation between the design variables and optimization objectives, and the Pearson correlation coefficient can be calculated by Eq. (7) to measure the correlation between the design variables and optimization objectives.

$$\rho_{X_i,Y_i} = \frac{N\sum X_iY_i - \sum X_i \sum Y_i}{\sqrt{N\sum X_i^2 - \left(\sum X_i\right)^2}\sqrt{N\sum Y_i^2 - \left(\sum Y_i\right)^2}} \quad (7)$$

where X_i denotes the parameter variables, Y_i the ith optimization objective, and N the number of samples. The sensitivity analysis results of the 10 design variables of the selected motor regarding average torque, torque ripple, and cogging torque are shown in Fig. 6.

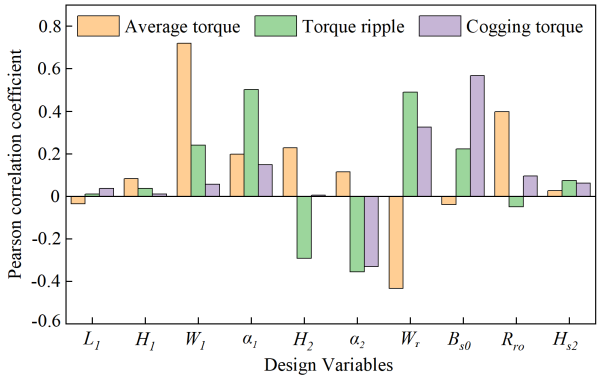

FIGURE 6. Pearson correlation coefficient.

Each design variable does not have the same degree of correlation with the optimization objective, and it is difficult to select the key design variables only based on the results of the corresponding correlation coefficients, so a comprehensive sensitivity analysis method is used to solve this problem. For SIHPMSM, the comprehensive sensitivity of the selected design variables can be expressed by Eq. (8).

$$S_{SIHPMSM}(x_i) = \omega_1 \cdot \left|S_{T_{avg}}(x_i)\right| + \omega_2 \cdot \left|S_{T_{rip}}(x_i)\right| + \omega_3 \cdot \left|S_{T_{cog}}(x_i)\right| \quad (8)$$

where x_i is the ith design variable, and $S_{T_{avg}}(x_i)$, $S_{T_{rip}}(x_i)$, and $S_{T_{cog}}(x_i)$ are the Pearson correlation coefficients of this design variable for the average torque, torque ripple, and cogging torque, respectively. The comprehensive sensitivity index of each design variable is shown in Fig. 7.

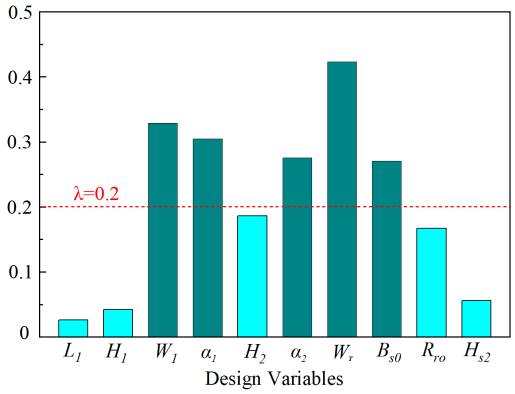

FIGURE 7. Comprehensive sensitivity index of design variables.

Considering the workload of the optimization design and calculation accuracy, the integrated sensitivity threshold λ is taken as 0.2 as the basis for judging the strong and weak sensitivity stratification of design variables, and the sensitivity stratification results of SIHPMSM-related design variables are shown in Table 3. For the design variables in the weak sensitivity layer, electromagnetic simulation analysis is performed using finite element analysis software to determine the optimal parameter values. For the strongly sensitive layer, an optimization algorithm will be used to optimize it.

TABLE 3. Stratification results of parameter variables.

Classifications	Design variables
Insensitive	L_1, H_1, H_2, R_{ro}, H_{s2}
Sensitive	W_1, α_1, α_2, W_T, B_{s0}

4.3. Multi-Objective Optimization

In this section, based on the design variable layering results in the previous subsection, the five parameter variables of the SIHPMSM strong correlation layer will be used as the optimization variables, and the multi-objective optimization algorithm combining GA-BP and NSGA-II will be used for the multi-objective optimal design of the motor in terms of the average torque, cogging torque, and torque ripple, and then the optimal solution will be selected from the set of the Pareto-optimal solutions, whose optimization flow is shown in Fig. 8.

4.3.1. Construction of the GA-BP Prediction Model

BP neural network is a branch of artificial neural networks. Its structure includes input layer, hidden layer, and output layer, and the signal is transmitted forward, with error back propagation as its main characteristics. BP neural network through the gradient descent method to guide and amend the weights and thresholds of the network to find out the optimal solution process will produce oscillation, network performance degradation, and the weights and thresholds are easy to fall into the

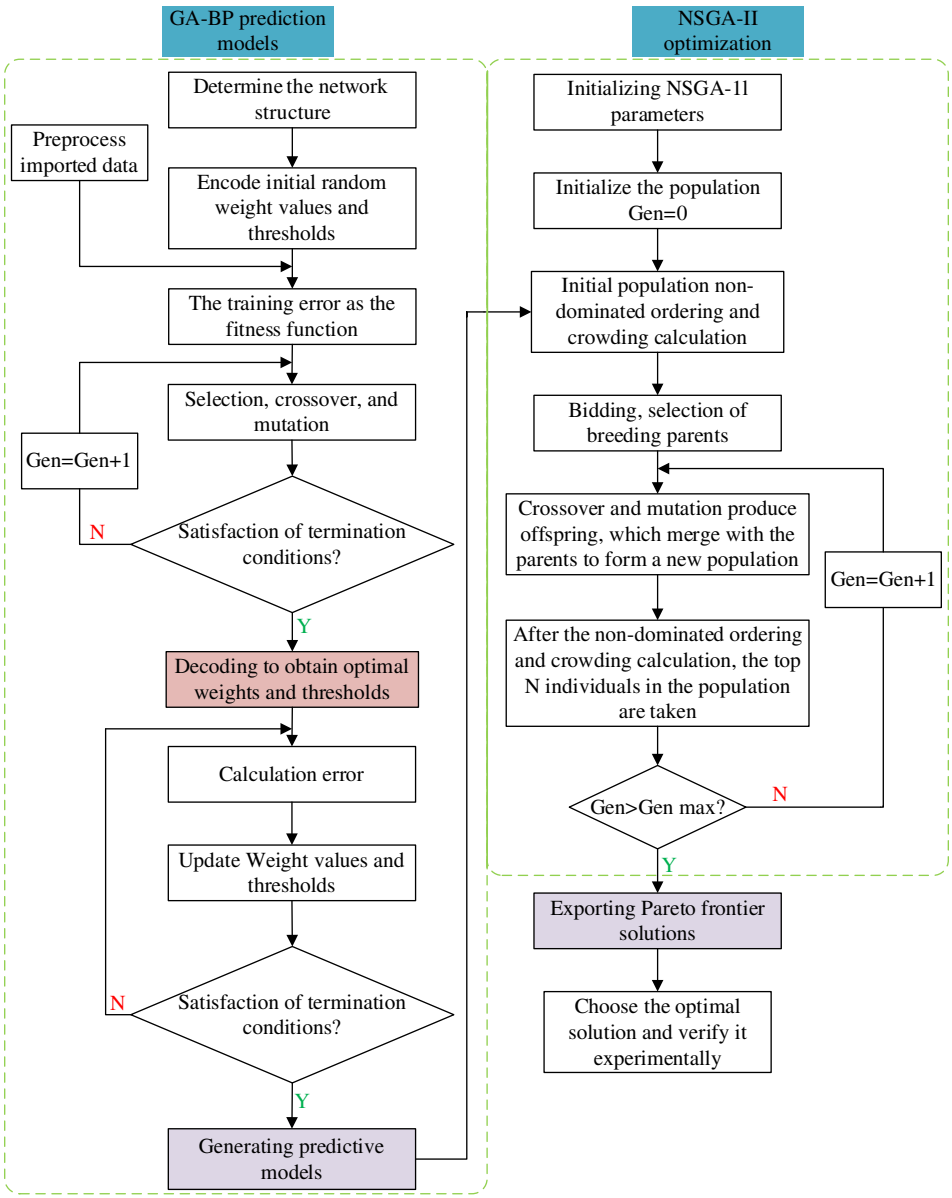

FIGURE 8. Optimization flowchart of GA-BP + NSGA-II.

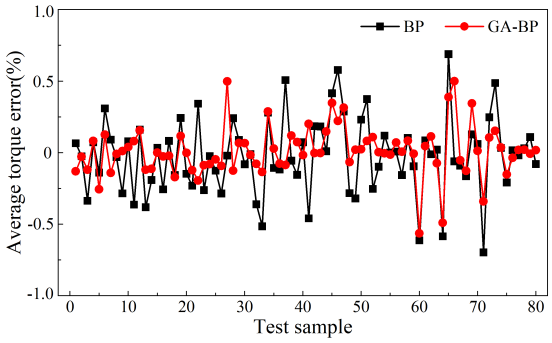

FIGURE 9. Prediction error of average torque.

local minima. Therefore, in this paper, GA is used to find the optimal weights and thresholds of each neuron to optimize the performance of the BP neural network to achieve the purpose of improving its prediction accuracy and generalization ability.

The number of training sets and test sets of GA-BP algorithm in this paper are taken as 320 and 80, respectively. After training and testing, the optimal fitting errors of average torque, torque ripple, and cogging torque are shown in Figs. 9, 10, and 11, respectively.

As can be seen from Figs. 9, 10, and 11, the prediction model after the GA-optimized BP neural network has a smaller error than the traditional BP neural network, and the associated error is shown in Table 4.

4.3.2. NSGA-II Based Optimization

Although the traditional NSGA is more uniform in the distribution of non-inferior optimal solutions than other multi-objective algorithms, due to the high computational complexity and time-consuming, Deb et al. proposed an improved non-dominated sorting genetic algorithm (NSGA-II) [21]. NSGA-II algorithm

TABLE 4. Comparison of GA-BP and BP neural network prediction model errors.

Optimization objectives	GA-BP model error		BP model error	
	maximum error	average error	maximum error	average error
T_{avg}	0.56%	0.12%	0.69%	0.2%
T_{rip}	4.73%	2.11%	14.9%	3.64%
T_{cog}	4.94%	2.48%	19.93%	4.08%

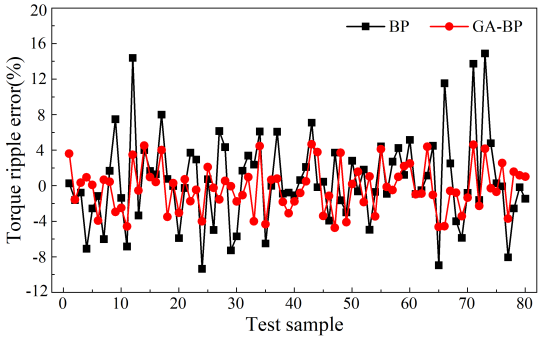

FIGURE 10. Prediction error of torque ripple.

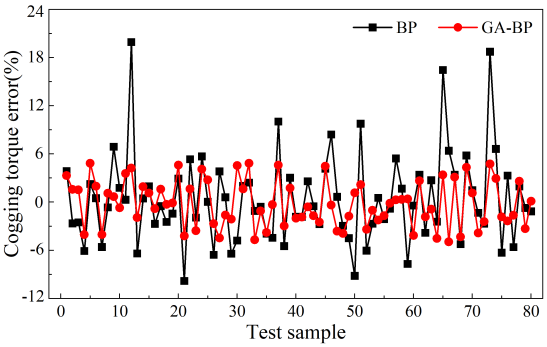

FIGURE 11. Prediction error of cogging torque.

using a fast non-dominated sorting strategy significantly reduces the computational time, reduces the computational cost, and ensures that good solutions are retained. The algorithm enhances the diversity of individuals in the Pareto domain through crowding and crowding comparison operators, which improves the global search capability of the algorithm.

NSGA-II takes the best prediction model of GA-BP as the optimization function and realizes multi-objective optimization by adjusting the main parameters of NSGA-II algorithm. The number of population iterations and the number of populations in the algorithm are set to 50 and 80, and the crossover and mutation probabilities are 0.8 and 0.2, respectively. Then, the optimization algorithm is run to get the solution set of the Pareto frontier, as shown in Fig. 12. The main objective of the optimization design in this paper is to minimize the torque ripple as much as possible when the average motor torque meets the performance requirements, and the cogging torque is within a reasonable range. The one marked with a red pentagram in Fig. 12 is selected as the optimal solution of the optimization objective. The initial and optimized values of the motor optimization variables are shown in Table 5, from which it can be seen that the design solution after multi-objective optimization can achieve the optimization objective and comply with the constraints, so as to obtain the topology that makes the SIHPMSM perform optimally.

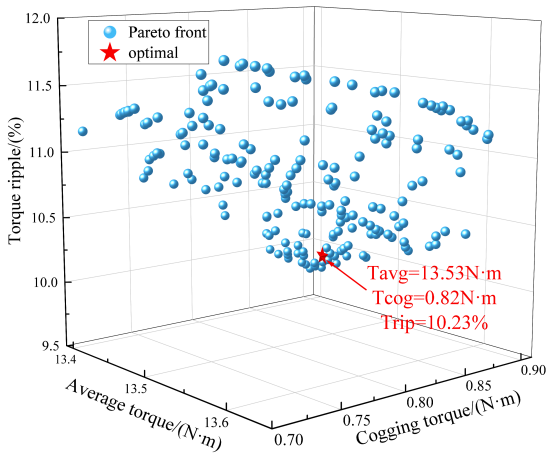

FIGURE 12. Pareto front.

4.4. Analysis of Optimization Results

In order to verify the effectiveness of the multi-objective optimization design method, simulation software is used to simulate and analyze the air-gap magnetic flux density, back-EMF, and torque characteristics of the SIHPMSM before and after optimization. Fig. 13 shows the magnetic field distribution of the optimized SIHPMSM under no-load condition, in which the left and right two semicircles are the magnetic density cloud and magnetic line distribution of this motor, respectively, and it can

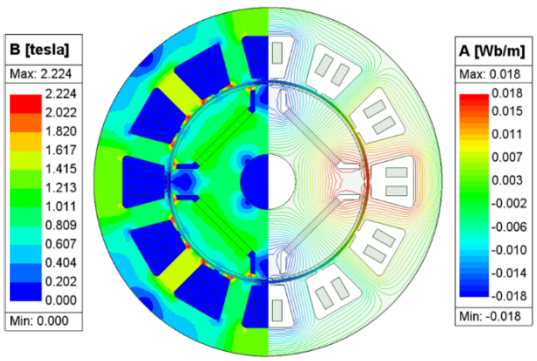

FIGURE 13. Cloud chart of magnetic flux density and distribu-tion map of magnetic field lines.

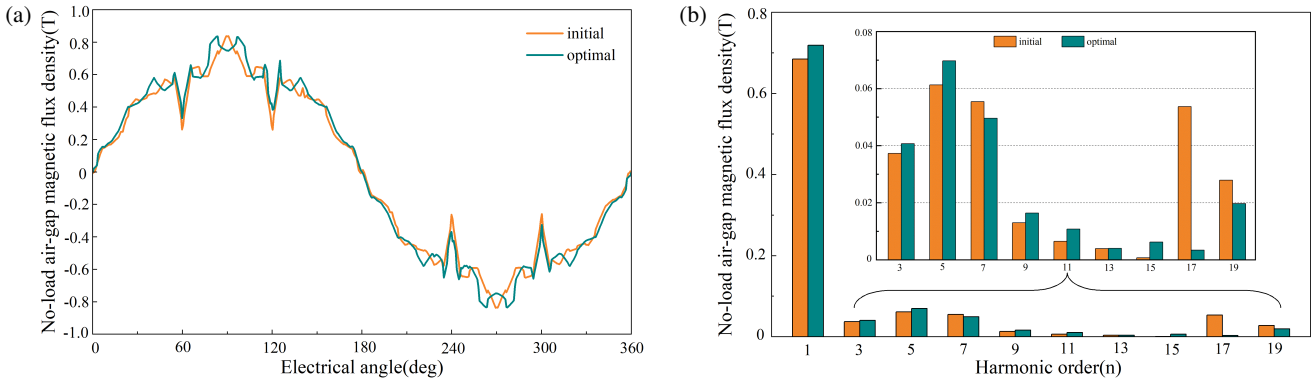

FIGURE 14. Comparison of initial and optimized air-gap magnetic flux densities, (a) eaveforms, (b) harmonic.

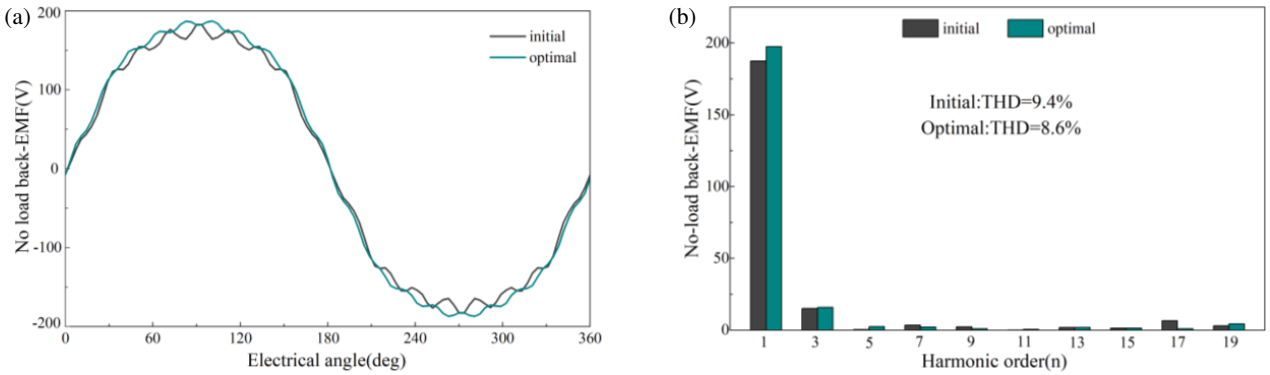

FIGURE 15. Comparison of initial and optimized no-load back EMF. (a) Waveforms. (b) Harmonic.

TABLE 5. Comparation of structural parameters before and after optimization.

Design Variables	Initial values	Optimal values
L_1	11.4 mm	13 mm
H_1	3.3 mm	3 mm
W_1	30.5 mm	32 mm
α_1	53.5 deg	53 deg
H_2	1.3 mm	1.4 mm
α_2	86 deg	88 deg
W_T	8.2 mm	9.6 mm
B_{s0}	2.6 mm	2.5 mm
R_{ro}	41.5 mm	41.6 mm
H_{s2}	16.5 mm	16.2 mm

be seen that the optimized motor has a higher flux density and a more uniform distribution of the magnetic lines, which indicates that the design is reasonable.

The no-load air-gap magnetic flux density waveform of SIHPMSM is shown in Fig. 14(a). From the figure, it can be seen that the optimized motor air-gap magnetic flux density amplitude is improved compared to the initial motor, and the air-gap magnetic flux density curve is smoother. Fig. 14(b) shows the comparison between the initial SIHPMSM and the optimized SIHPMSM in terms of the harmonic content of the airgap magnetic flux density, from which it can be seen that the fundamental amplitude of this motor after optimization has been improved; the 7th, 17th, and 19th harmonics have been reduced; the 17th harmonic has decreased more significantly. The air-gap magnetic flux density harmonic distortion rate of this motor decreases from the initial 16.06% to 13.78%, which is a decrease of 14.2%

The no-load back-EMF waveforms as well as the harmonic content plots of the SIHPMSM are shown in Figs. 15(a) and (b), respectively. From Fig. 15(a), it can be seen that the optimized motor back-EMF waveform is more sinusoidal than the initial one, and the amplitude is higher. From Fig. 15(b), it can be seen that the amplitude of the fundamental waveform of the SIHPMSM increases from the initial 187.5 V to 197.5 V, an increase of 5.3%.

Figures 16 and 17 show the output torque of the SIHPMSM under loaded and no-load conditions, respectively. It can be seen from Fig. 16 that under the rated load condition, the initial average torque of the motor is 12.90 N · m, and it becomes 13.53 N · m after optimization. The average torque after optimization is 4.88% higher than the initial one. The initial torque ripple of the motor is 17.23%, and it drops to 10.23% after optimization. The torque ripple after optimization is 40.63% lower than the initial one. It can be known from Fig. 17 that under the no-load condition, the initial peak-to-peak value of the cogging torque of the motor is 0.91 N · m, and it is 0.82 N · m after optimization. The peak-to-peak value of the cogging torque after optimization is 9.89% lower than the initial one.

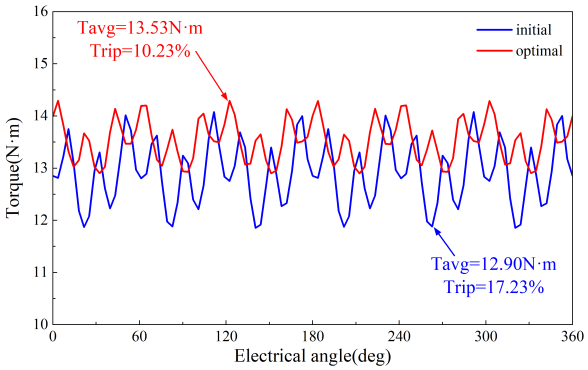

FIGURE 16. Initial and optimized torques under load condition.

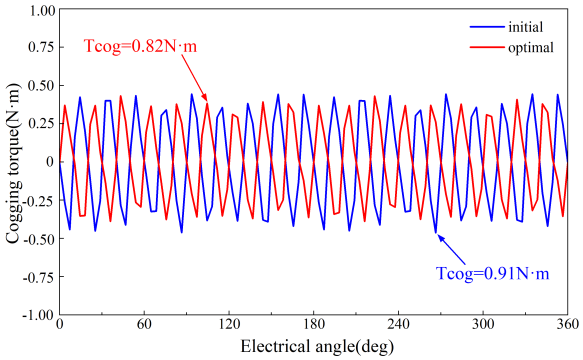

FIGURE 17. Initial and optimized torques under no-load condition.

5. CONCLUSION

In this paper, two aspects of motor topology and parameter optimization are used to improve the performance of permanent magnet synchronous motors. For the former, a new rotor topology with a mixture of eccentric surface-mounted poles and interior poles is proposed, which can effectively weaken the harmonic distortion rate of the motor's back-EMF and the harmonic distortion rate of the air-gap magnetic flux density. Moreover, compared with SPMSM and IPMSM, SIHPMSM with the new rotor topology has the advantages of good weak magnetic performance and higher torque output at the same time. For the latter, the initial weights and thresholds of the BP neural network are firstly optimized by using GA to obtain the prediction model, which solves the problem that traditional BP neural network is easy to fall into the local minima and improves the prediction accuracy of the prediction model. Then, NSGA-II is used to carry out multi-objective optimization to obtain the Pareto front solution set and select the optimal solution from it. Finally, the performances of the SIHPMSM before and after optimization are compared by finite element simulation experiments, and the results show that the average torque of the optimized motor increases by 4.88%; the torque ripple decreases by 40.63%; and the cogging torque decreases by 9.89% compared to the initial motor.

REFERENCES

[1] Song, C.-H., I.-S. Song, H.-S. Shin, C.-H. Lee, and K.-C. Kim, "A design of IPMSM for high-power electric vehicles with wide-field-weakening control region," *IEEE Transactions on Magnetics*, Vol. 58, No. 2, 1–5, 2021.

[2] Cho, S.-K., K.-H. Jung, and J.-Y. Choi, "Design optimization of interior permanent magnet synchronous motor for electric compressors of air-conditioning systems mounted on EVs and HEVs," *IEEE Transactions on Magnetics*, Vol. 54, No. 11, 1–5, 2018.

[3] Kim, D.-H., K. S. Kim, I.-J. Yang, J. Lee, and W.-H. Kim, "Alternative bridge spoke permanent magnet synchronous generator design for wind power generation systems," *IEEE Access*, Vol. 9, 152 819–152 828, 2021.

[4] Chai, F., Y. Li, P. Liang, and Y. Pei, "Calculation of the maximum mechanical stress on the rotor of interior permanent-magnet synchronous motors," *IEEE Transactions on Industrial Electronics*, Vol. 63, No. 6, 3420–3432, 2016.

[5] Wang, X.-Y., X.-Y. He, and P. Gao, "Research on electromagnetic vibration and noise reduction method of V type magnet rotor permanent magnet motor electric vehicles," *Proceedings of the CSEE*, Vol. 39, No. 16, 4919–4926, 2019.

[6] Wang, D., C. Peng, B. Wang, Z. Feng, and F. Zhang, "Research on a novel interior permanent magnet machine with segmented rotor to mitigate torque ripple and electromagnetic vibration," *Proceedings of the CSEE*, Vol. 42, No. 14, 5289–5299, 2022.

[7] Chai, W. and B.-I. Kwon, "A magnetic pole modulation method on surface permanent magnet machines for high performances with different magnetization," *IEEE Access*, Vol. 7, 79 839–79 849, 2019.

[8] Yang, Y.-P. and M.-T. Peng, "A surface-mounted permanent-magnet motor with sinusoidal pulsewidth-modulation-shaped magnets," *IEEE Transactions on Magnetics*, Vol. 55, No. 1, 1–8, 2018.

[9] Xie, X., C. Liao, and Z. Zhang, "Design considerations of high-speed PMSM with nonuniform two-segment Halbach magnet array," *IEEE Transactions on Magnetics*, Vol. 60, No. 9, 1–6, 2024.

[10] Chen, Z., C. Xia, Q. Geng, and Y. Yan, "Modeling and analyzing of surface-mounted permanent-magnet synchronous machines with optimized magnetic pole shape," *IEEE Transactions on Magnetics*, Vol. 50, No. 11, 1–4, 2014.

[11] Xie, B., Y. Zhang, Z. Xu, F. Zhang, and W. Liu, "Review on multidisciplinary optimization key technology of electrical machine based on surrogate models," *Transactions of China Electrotechnical Society*, Vol. 37, No. 20, 5117–5143, 2022.

[12] Chen, H. and C. H. T. Lee, "Parametric sensitivity analysis and design optimization of an interior permanent magnet synchronous motor," *IEEE Access*, Vol. 7, 159 918–159 929, 2019.

[13] Wang, X., Y. Fan, X. Lu, Q. Chen, and C. H. T. Lee, "Multiobjective optimization of a dual stator brushless hybrid excitation motor based on response surface model and NSGA 2," *IEEE Transactions on Industry Applications*, Vol. 58, No. 5, 6105–6114, 2022.

[14] Chu, J., H. Cheng, J. Sun, C. Peng, and Y. Hu, "Multi-objective optimization design of hybrid excitation double stator permanent magnet synchronous machine," *IEEE Transactions on Energy Conversion*, Vol. 38, No. 4, 2364–2375, 2023.

[15] Hua, Y., Y. Liu, W. Pan, X. Diao, and H. Zhu, "Multi-objective optimization design of bearingless permanent magnet synchronous motor using improved particle swarm optimization algorithm," *Proceedings of the CSEE*, Vol. 43, No. 11, 4443–4451, 2023.

[16] Guo, X., N. W. Gong, Q. J. Wang, Y. Weng, and T. Wu, "Optimization electrifying strategy of permanent magnet spherical

motor based on random forests," *Control Engineering of China*, Vol. 28, No. 6, 1100–1107, 2021.

[17] Bao, Y., Y. Cheng, and J. Tian, "Multi-objective optimization of electromagnetic structure of high-speed permanent magnet synchronous motor for vehicles," *Machine Tool and Hydraulics*, Vol. 52, No. 20, 42–47, 2024.

[18] Kwon, M.-S. and D.-K. Lim, "A study on the optimal design of PMa-SynRM for electric vehicles combining random forest and genetic algorithm," *IEEE Access*, Vol. 11, 52 357–52 369, 2023.

[19] Asanuma, J., S. Doi, and H. Igarashi, "Transfer learning through deep learning: Application to topology optimization of electric motor," *IEEE Transactions on Magnetics*, Vol. 56, No. 3, 1–4, 2020.

[20] Son, B., J.-S. Kim, J.-W. Kim, Y.-J. Kim, and S.-Y. Jung, "Adaptive particle swarm optimization based on kernel support vector machine for optimal design of synchronous reluctance motor," *IEEE Transactions on Magnetics*, Vol. 55, No. 6, 1–5, 2019.

[21] Deb, K., A. Pratap, S. Agarwal, and T. Meyarivan, "A fast and elitist multiobjective genetic algorithm: NSGA-II," *IEEE Transactions on Evolutionary Computation*, Vol. 6, No. 2, 182–197, 2002.